Pepler. *Journal of Southern Hemisphere Earth Systems Science* (2016) 66:361-379. DOI: 10.22499/3.6604.001

Seasonal climate summary southern hemisphere (summer 2015-16): strong El Niño peaks and begins to weaken

Acacia S. Pepler[1]

[1] Bureau of Meteorology, Sydney, Australia

(Manuscript received September 2016; accepted September 2016)

Southern hemisphere circulation patterns and associated anomalies for austral summer 2015-16 are reviewed, with an emphasis on the tropical Pacific as well as Australian rainfall and temperatures. Following the peak of El Niño in November 2015, summer 2015-16 featured continued near-record El Niño conditions in the tropical Pacific but saw the emergence of cooler subsurface waters in the equatorial Pacific. A moderate Madden Julian Oscillation (MJO) pulse and positive Southern Annular Mode (SAM) ontributed to average to above average rainfall across much of Australia, while the Maritime Continent and parts of far northern Australia saw continued below average rainfall.

Sea surface temperatures during summer 2015-16 were the warmest on record for the southern hemisphere oceans, with very warm ocean temperatures in the Indian Ocean and Australian region, including the warmest summer sea surface temperatures on record around Tasmania. Air temperatures were also warmer than normal across Australia throughout the season, with a significant heatwave in southeast Australia during December.

1. Introduction

This summary reviews the southern hemisphere and equatorial climate patterns for austral summer 2015-16, with particular attention given to the Australasian and Pacific regions. The main sources of information for this report are analyses prepared by the Bureau of Meteorology.

2. Pacific Basin climate indices

2.1 Southern Oscillation Index

The Troup Southern Oscillation Index[1] (SOI) for the period January 2012 to February 2016 is shown in Figure 1, together with a five-month weighted moving average. Following a period of negative SOI values during 2014, a strong El Niño event became established during winter and spring 2015. The SOI weakened slightly during late 2015, with a monthly value of -9.1 in December 2015. However, the SOI returned to very strong values during late summer, with a monthly value of -19.7 in both January and February.

The seasonal average SOI was -16.2, the strongest summer SOI since summer 1997-8 (-17.3) and the fifth-largest summer SOI since records began in 1876. Summer mean sea level pressure (MSLP) values were well above average in Darwin,

[1] The Troup Southern Oscillation Index (Troup 1965) used in this article is ten times the standardised monthly anomaly of the difference in mean-sea-level pressure (MSLP) between Tahiti and Darwin. The calculation is based on a sixty-year climatology (1933–1992). The Darwin MSLP is provided by the Bureau of Meteorology, and the Tahiti MSLP is provided by Météo France inter-regional direction for French Polynesia.

Corresponding author: Acacia S. Pepler, Bureau of Meteorology, PO Box 413, Darlinghurst NSW 1300 Australia
Email: a.pepler@bom.gov.au

with the mean January sea level pressure 3.8 hPa above average, the highest January sea level pressure on record, and anomalies of +2.1 in February and +0.3 in December. The monthly MSLP anomalies for Tahiti were -1.5 in December, -0.2 in January, and -2.0 in February.

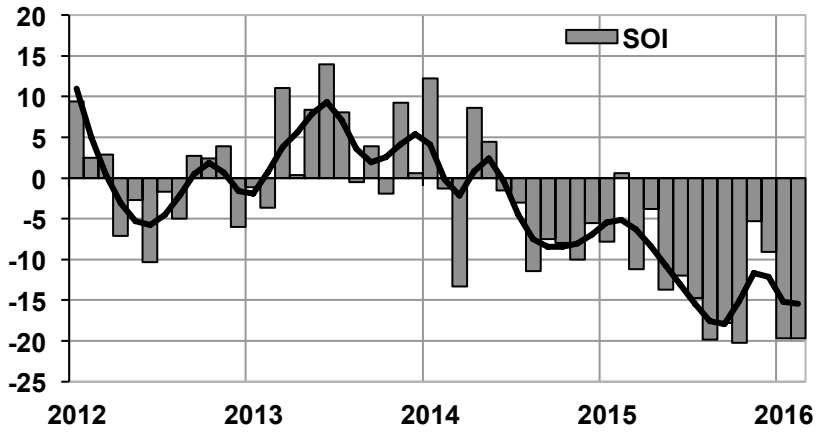

Figure 1 Southern Oscillation Index, from January 2012 to February 2016, together with a five-month binomially weighted moving average. Means and standard deviations used in the computation of the SOI are based on the period 1933–1992.

2.2 Composite monthly ENSO indices

5VAR[2] is a composite monthly ENSO index, calculated as the standardised amplitude of the first principal component of monthly Darwin and Tahiti MSLP[3] and monthly NINO3, NINO3.4 and NINO4 sea-surface temperatures[4] (SSTs). Monthly 5VAR values for the period January 2012 to February 2016, with a weighted three-month moving average, are shown in Figure 2. Persistently positive (negative) values in excess of one standard deviation typically indicate El Niño (La Niña). Following record-high 5VAR values during both winter and spring, values began to decrease during summer 2015-16, with monthly values decreasing from 2.1 in December to 1.3 in both January and February. The seasonal mean 5VAR index was 1.5, the fourth-highest summer value on record behind 1982-3, 1997-8 and 1991-2.

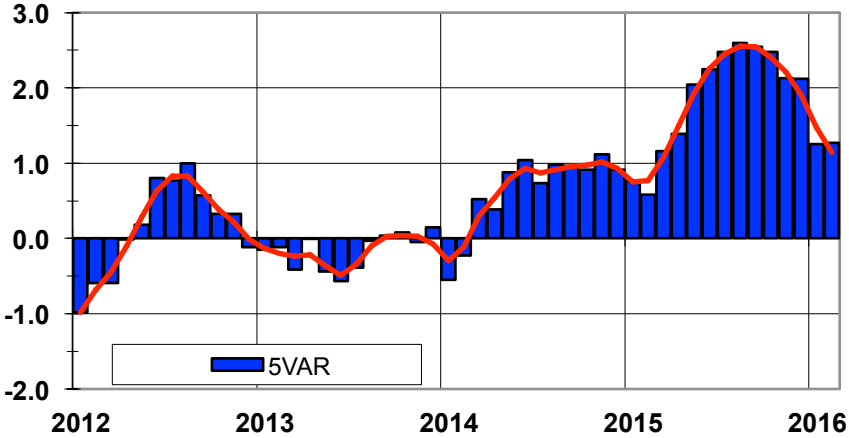

Figure 2 5VAR composite standardised monthly ENSO index from January 2012 to February 2016, together with a weighted three-month moving average. See text for details.

[2] ENSO 5VAR was developed at the Bureau's National Climate Centre and is described in Kuleshov et al. 2009. The principal component analysis and standardisation of this ENSO index is performed over the period 1950–1999.
[3] MSLP data obtained from http://www.bom.gov.au/climate/current/soihtm1.shtml. Tahiti MSLP is provided by Météo France inter-regional direction for French Polynesia.
[4] SST indices obtained from ftp://ftp.cpc.ncep.noaa.gov/wd52dg/data/indices/sstoi.indices.

The Multivariate ENSO Index[5] (MEI), produced by the Physical Sciences Division of the Earth Systems Research Laboratory (formerly known as the US Climate Diagnostics Center), is derived from a number of atmospheric and oceanic parameters calculated as a two-month mean (Wolter and Timlin 1993, 1998). As with 5VAR, large negative anomalies in the MEI are usually associated with La Niña and large positive anomalies indicate El Niño. The December-January (+2.2) and January-February (+2.1) MEI values are also the third-highest values on record, following the El Niños of 1982-3 and 1997-8.

2.3 Outgoing long-wave radiation

Outgoing long-wave radiation (OLR) over the equatorial Pacific Ocean is a good indicator of changes in tropical convection patterns, with El Niño (La Niña) years associated with suppressed (enhanced) convection in the western equatorial Pacific and enhanced (suppressed) convection near the Date Line. During summer 2015-16, the standardised monthly OLR anomaly[6] for the equatorial region between 5°S and 5°N and 160°E to 160°W was -35.4 W m-2. This is the strongest summer OLR anomaly since records began in 1979, slightly ahead of summer 1986-7 (-34.9 W m-2) and 2009-10 (-34.5 W m-2), and stronger than the anomalies in the previous strong El Niño events in 1997-8 (-11.2 W m-2) and 1982-3 (-14.4 W m-2). Anomalies were at least 1.9 standard deviations below average in all three months, indicating very strongly enhanced convection in that region throughout summer.

Figure 3 shows the spatial pattern of seasonal OLR anomalies. Strongly positive OLR anomalies are present across the Maritime Continent, northern Australia, and the subtropical convergence zone, corresponding to reduced rainfall in these regions, with strongly enhanced convection further eastward along the equator. OLR was generally negative across the remainder of Australia, coinciding with average to above average rainfall. However, due to drift in the NOAA-18 satellite orbit, a negative OLR bias is emerging over subtropical land areas, with a bias of around 5 W m-2 estimated during spring 2015 (Martin, D. J. 2016)

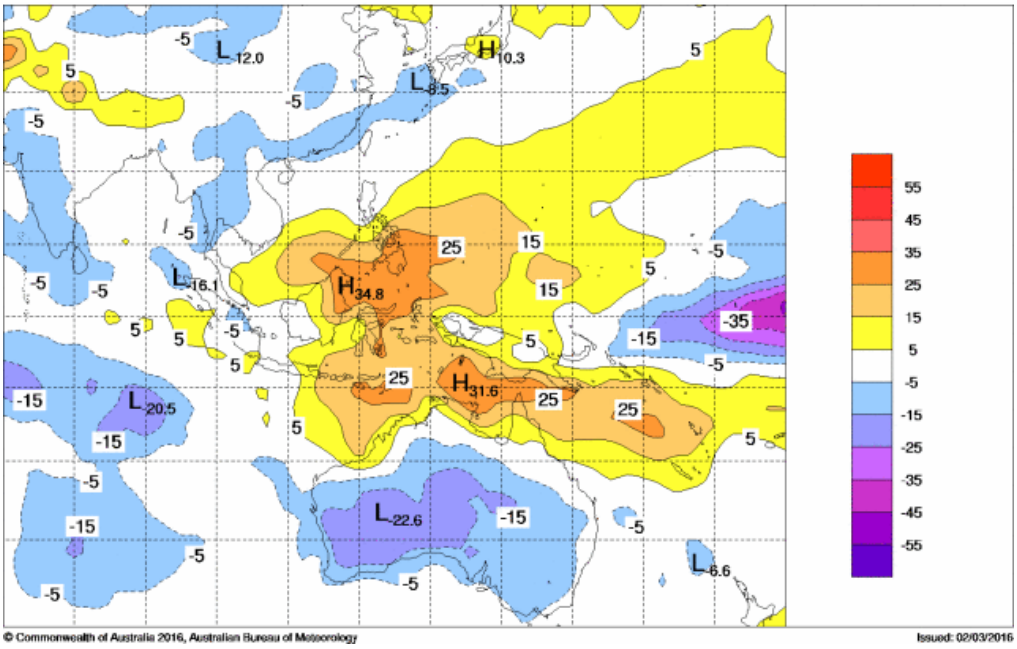

Figure 3 OLR anomalies for summer 2015-16 (W m−2). Base period 1979–2000. The mapped region extends from 40°S to 40°N and from 70°E to 180°E.

[5] Multivariate ENSO Index obtained from http://www.esrl.noaa.gov/psd/people/klaus.wolter/MEI/table.html. The MEI is a standardised anomaly index described in Wolter and Timlin 1993, and 1998

[6] Obtained from http://www.cpc.ncep.noaa.gov/data/indices/olr

2.4 Madden-Julian Oscillation

The Madden–Julian Oscillation (MJO) can be characterised as a burst of tropical cloud and rainfall which develops in the Indian Ocean and propagates eastwards into the Pacific Ocean (Madden and Julian 1971, 1972, 1994). A typical cycle of the MJO lasts for between 30 and 60 days, with active phases associated with eastward-moving areas of increased tropical convection as well as broader impacts outside the tropics (e.g. Donald et al. 2006). The MJO can be monitored using patterns of tropical OLR anomalies and the Real-time Multivariate MJO (RMM) index described by Wheeler and Hendon (2004).

During summer 2015-16, cloudiness remained well below average across the Maritime Continent (90-160°E), with persistent westerly wind anomalies (Figure 4). This is typical of El Niño conditions. However, there were two clear bursts of eastward-moving convection during the summer. The MJO was active for most of summer (Figure 5), with a pulse originating in phase 4 during December and making a full circuit before ending in phase 8 at the end of February.

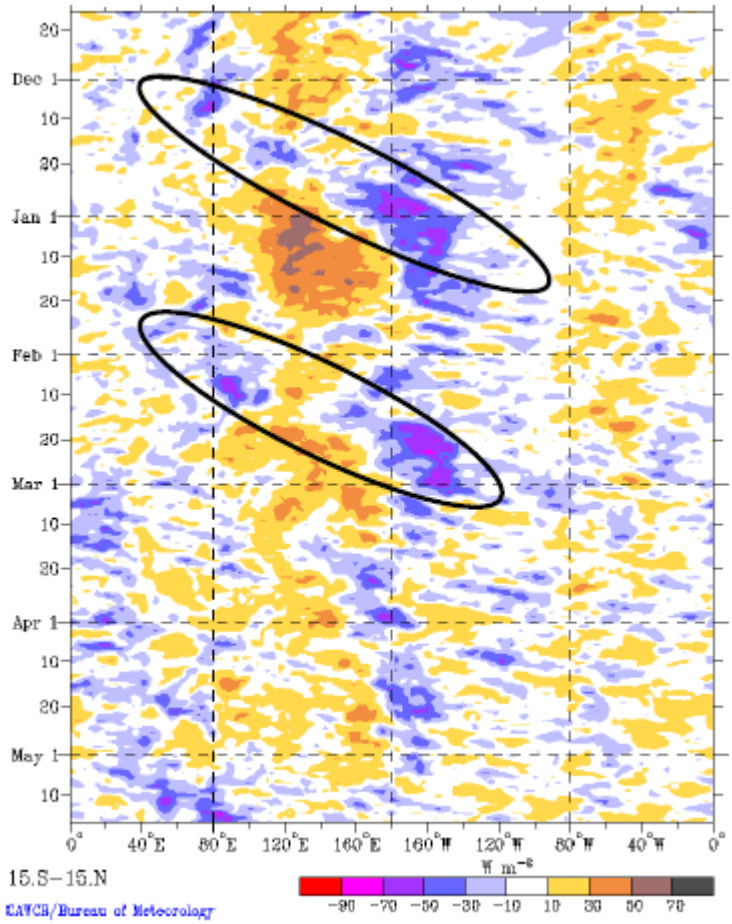

Figure 4 Time-longitude section of daily-averaged OLR anomalies, averaged for 15ºS to 15ºN, for the period November 2015 through to May 2016. Anomalies are with respect to a base period of 1979–2010.

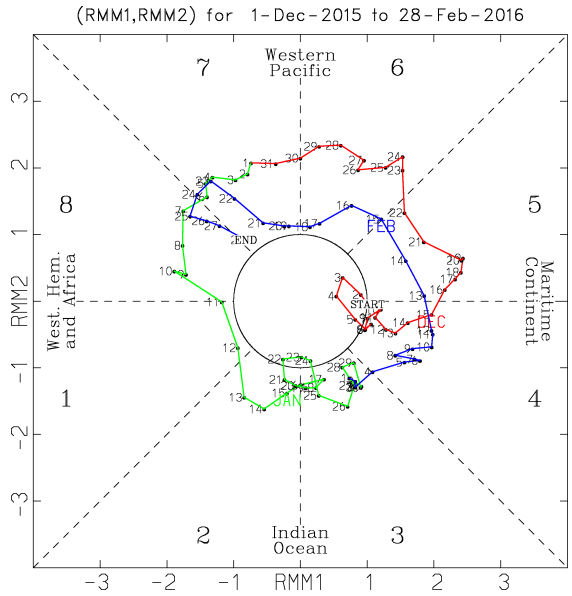

Figure 5 Phase-space representation of the MJO index for summer 2015-16. Daily values are shown with December in red, January in green and February in blue.

3. Oceanic patterns

3.1 Sea-surface temperatures

Sea surface temperatures (SSTs) were warmer than average across much of the globe during summer 2015-16 (Figure 6). For both the global and southern hemisphere oceans, summer SSTs were the warmest on record, with the average summer SST in the southern hemisphere 0.77 °C above the 1901-2000 average and 0.15 °C above the previous record, set in summer 2009-10[7].

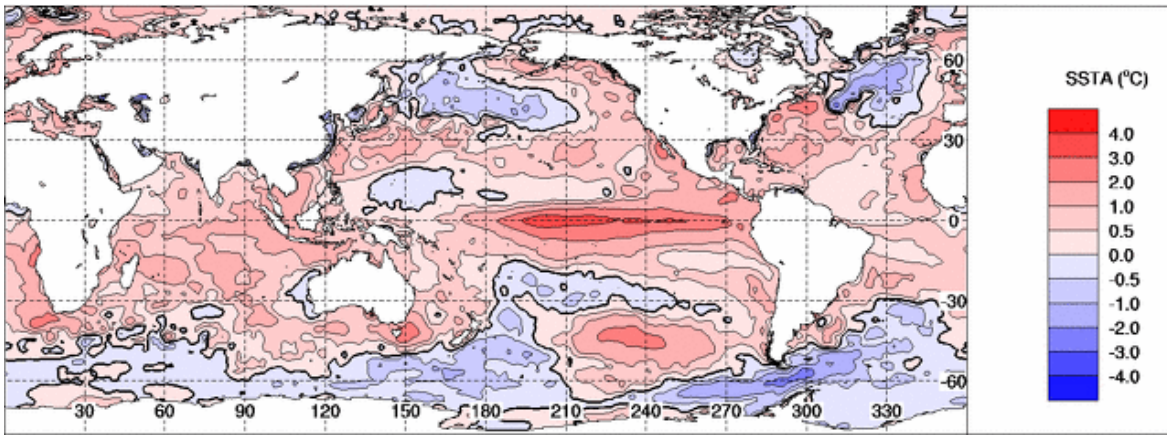

Figure 6 Anomalies of SST for summer 2015-16 (°C), from the US National Oceanic and Atmospheric Administration (NOAA) Optimum Interpolation analyses (Reynolds et al. 2002). The base period is 1981-2010.

[7] SST anomalies available from https://www.ncdc.noaa.gov/monitoring-references/faq/anomalies.php

In the key NINO3.4[8] region in the central tropical Pacific, summer SSTs were 2.6 °C above normal, similar to the record El Niño years of 1997-8 (+2.5 °C) and 1982-3 (+2.6 °C), following a peak temperature anomaly of +2.95 °C during November 2015. Warm SSTs were also present across most of the Indian Ocean and the Australian region, with record-warm summer SSTs in the Gulf of Carpentaria and in the waters surrounding Tasmania (Figure 7). Warm sea surface temperatures in the Indian Ocean have now persisted for six years following their emergence during the 2010-11 La Niña (Ganter 2011, Lee et al. 2015).

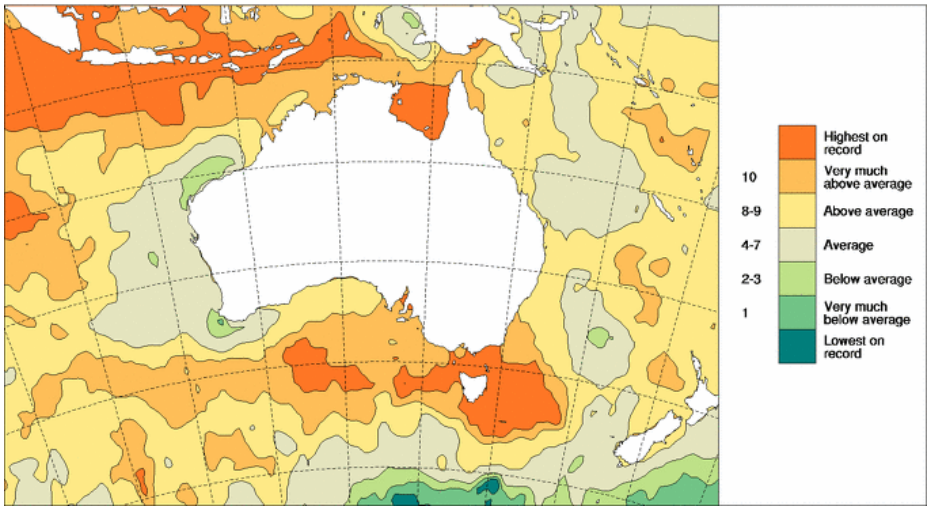

Figure 7 SST deciles in the Australian region for summer 2015-16 (°C).

3.2 Subsurface patterns

Figure 8 shows a cross-section of monthly vertical temperature anomalies from November 2015 to February 2016, from 120°E to 80°W and to a maximum depth of 400 m across the equatorial Pacific Ocean[9]. In terms of subsurface waters, the 2015-16 El Niño heat extent peaked during November 2015, with a large area of water in both the surface and subsurface with temperatures more than 4 °C above average. Over the summer, this pool of warm water shrank, with subsurface ocean temperature anomalies closer to 2 °C above average by the end of February despite little change in surface temperature anomalies. Meanwhile, a pool of cool water below the surface in the western Pacific grew and moved eastward during the season, with a layer of relatively cool water underneath the warmer waters in the central Pacific by the end of February.

The equatorial thermocline is the region where the vertical temperature gradient between warm surface waters and cold deep-ocean water is greatest, and can be approximated using the depth of the 20 °C isotherm. Positive (negative) anomalies correspond to a deeper (shallower) thermocline, with a deeper thermocline associated with suppressed upwelling and warming sea surface temperatures. Shifts in the depth of the 20 °C isotherm can thus provide an indicator of subsequent changes in SSTs.

[8] NINO3.4 available from ftp://ftp.cpc.ncep.noaa.gov/wd52dg/data/indices/sstoi.indices
[9] http://www.bom.gov.au/oceanography/oceantemp/pastanal.shtml

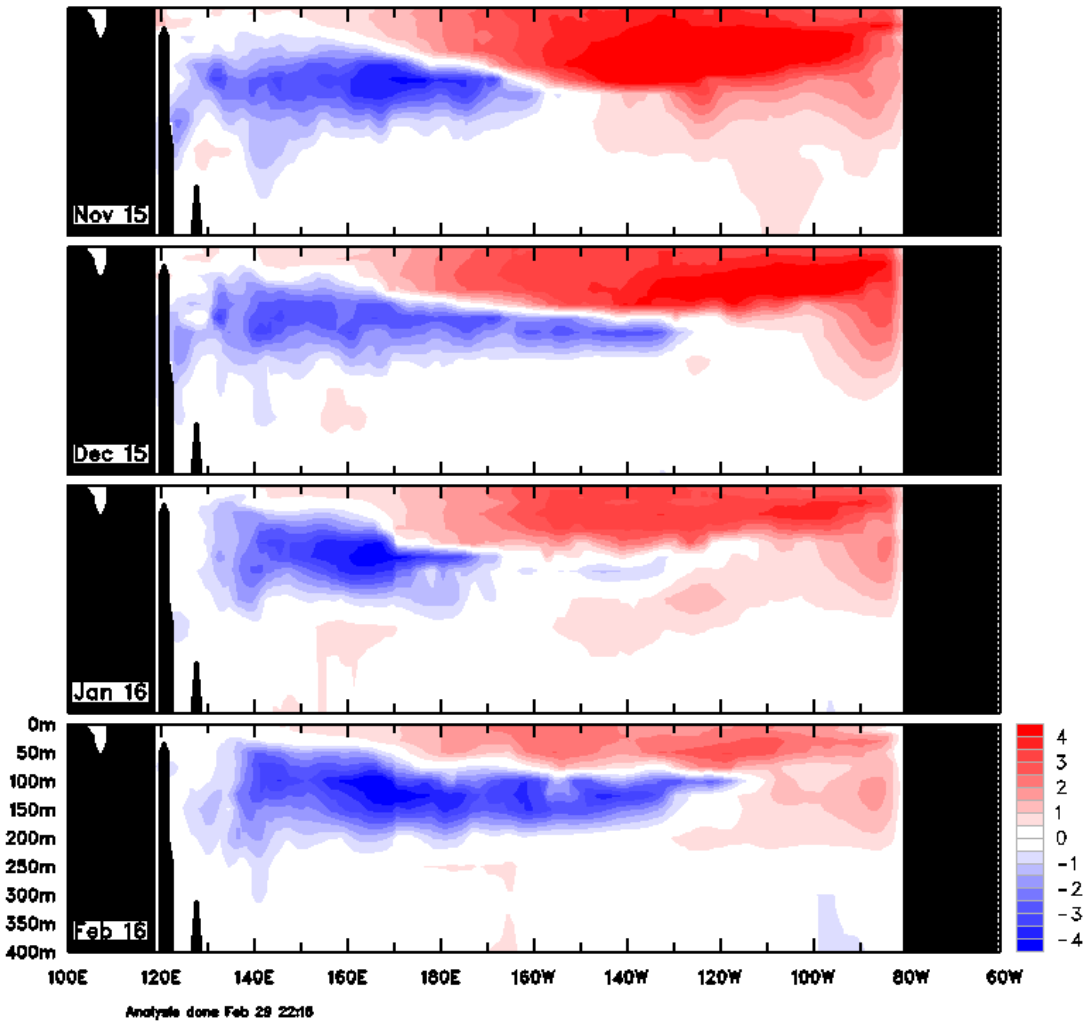

Figure 8 Four-month November 2015 to February 2016 sequence of vertical sea subsurface temperature anomalies at the equator for the Pacific Ocean. The contour interval is 0.5 °C. (Plot obtained from the Bureau of Meteorology at http://www.bom.gov.au/oceanography/oceantemp/pastanal.shtml.

Figure 9 is a Hovmöller diagram for the equatorial 20 °C isotherm depth anomaly between January 2014 and February 2016, obtained from NOAA's TAO Project Office[10]. The beginning of December saw an almost flat thermocline (Figure 10), a hallmark of a strong El Niño event, with cooler waters in the west and warmer waters in the east. Consistent with Figure 8, the development of cooler subsurface waters in the western equatorial Pacific during summer 2015-16 can be seen, with the 20 °C isotherm 20 m shallower than normal across the western third of the Pacific in December 2015. An upwelling Kelvin wave crossed the Pacific during summer, shifting the cooler water eastwards, and helping to weaken the positive isotherm height anomalies that had developed in the eastern Pacific over the course of the 2015-16 El Niño.

[10] http://www.pmel.noaa.gov/tao/jsdisplay/

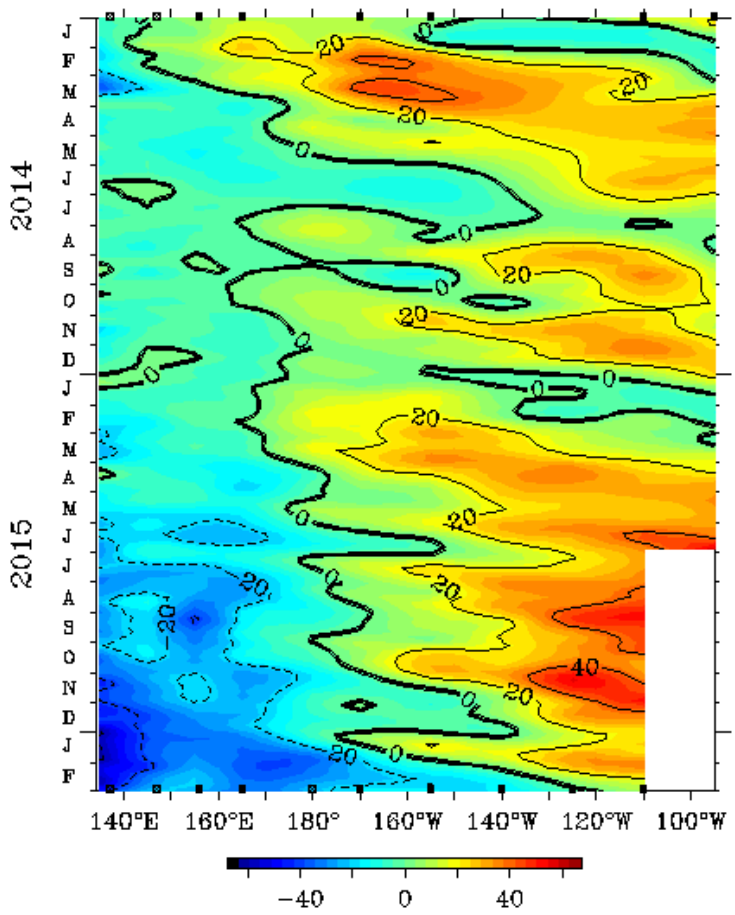

Figure 9 Time-longitude section of the monthly anomalous depth of the 20 °C isotherm at the equator (2ºS to 2ºN) for January 2014 to February 2016. (Plot obtained from the TAO Project Office)

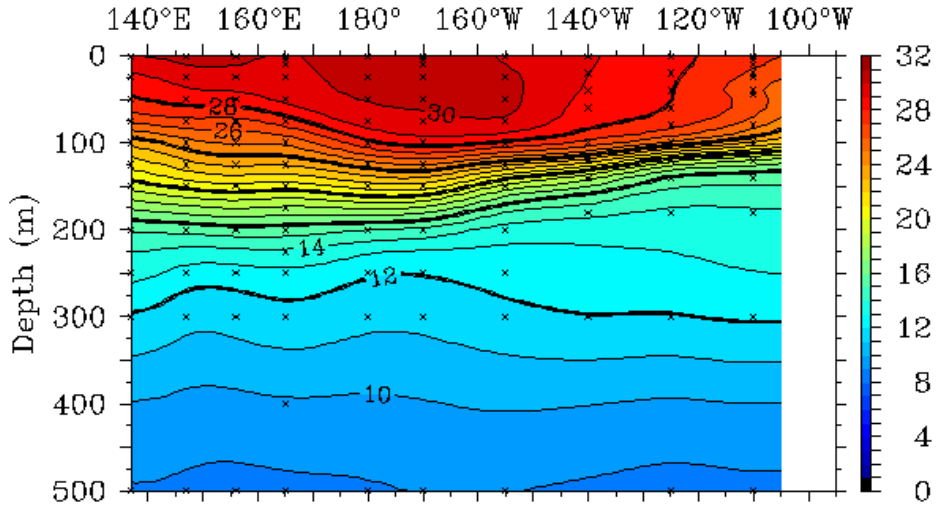

Figure 10 Mean subsurface ocean temperatures (°C) for 2°S to 2°N over the five days 30 November – 4 December 2015. Plot obtained from the TAO Project Office

4. Atmospheric patterns

4.1 Surface analyses

The southern hemisphere mean sea level pressure (MSLP) anomalies during summer 2015-16 are shown in Figure 11, relative to a 1979-2000 climatology. Pressure was abnormally low surrounding Antarctica, out to around 60°S, as well as over much of the central and eastern Pacific Ocean and in parts of the southern Indian Ocean. In comparison, pressure was relatively high over the Australian region and the south Atlantic, with anomalies of up to +4.43 hPa to the southwest of Australia, while an area of high pressure west of Chile was up to 5.72 hPa above normal. Over the Australian east coast (at 145-150°E longitudes), the subtropical ridge was located abnormally southward for summer, at a latitude of 39.7°S, while the average intensity was 1.3 hPa above the long-term average (Drosdowsky 2005).

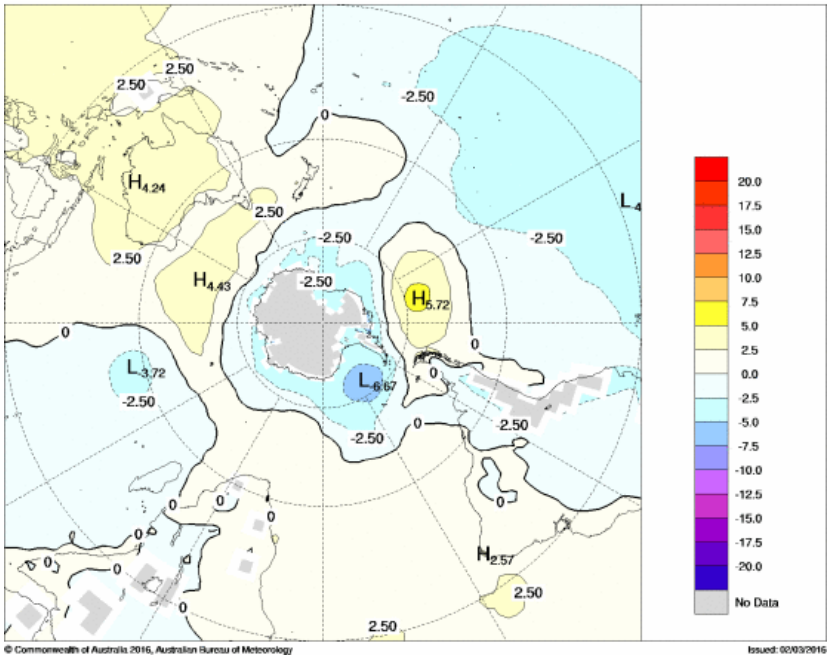

Figure 11 Summer 2015-16 MSLP anomalies (hPa) from the 0000UTC daily analyses of the Bureau of Meteorology's Global Assimilation and Prognosis (GASP) model, compared to a 1979–2000 climatology obtained from the National Centers for Environmental Prediction (NCEP2) Reanalysis data (Kanamitsu et al. 2002). Areas of elevated topography are shown with grey shading.

4.2 Mid-tropospheric analyses

The 500 hPa geopotential height is an indicator of the steering of surface synoptic systems across the southern hemisphere. During summer 2015-16, the 500 hPa geopotential height anomalies (Figure 11) were broadly similar to the MSLP anomalies shown above, with regions of below-average geopotential height over Antarctica and above average geopotential height in the Australian region and south Atlantic. The strongest local maxima was off the southwest coast of Chile, with heights 90.4 m above normal, while the strongest minima were to the east and west of the Antarctic Peninsula at close to -60 gpm.

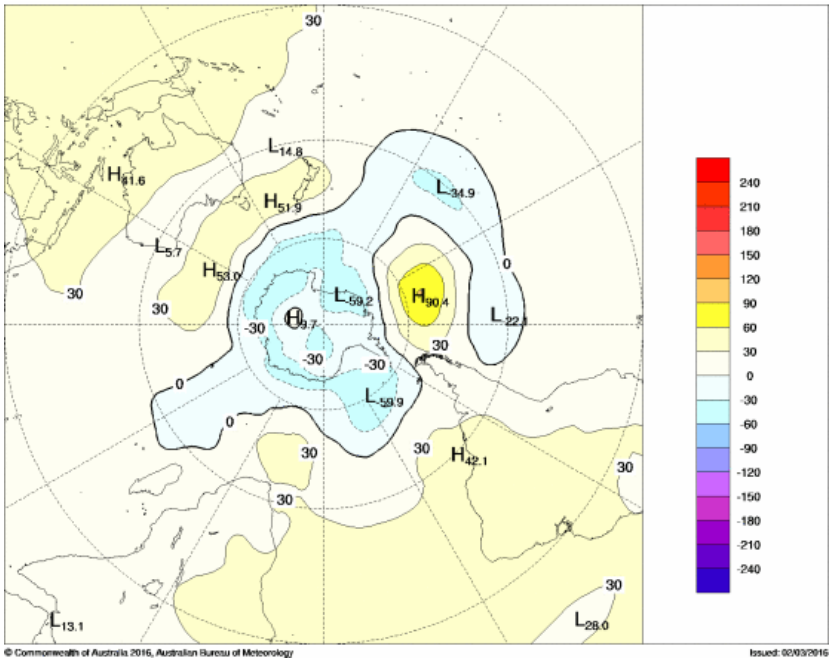

Figure 12 Summer 2015-16 500 hPa mean geopotential height anomalies (gpm), from a 1979–2000 climatology.

4.3 Southern Annular Mode

The Southern Annular Mode (SAM), also known as the Antarctic Oscillation (AAO), describes north-south shifts in the location of the belt of strong westerly winds in the middle to high latitudes of the southern hemisphere. Positive SAM is associated with negative MSLP anomalies near Antarctica and positive anomalies in the mid-latitudes, as the main belt of westerly winds moves polewards. During summer, positive SAM is associated with higher rainfall in much of southeast Australia, due to an enhancement of the moist easterly winds which provide much of the rainfall to southeast Australia during this season (Hendon et al. 2007, Rakich et al. 2008).

The daily SAM values during summer 2015-16 are shown in Figure 13, as given by NOAA's Climate Prediction Center. SAM was variable during December, with a monthly average anomaly close to 0. However, SAM, was consistently positive during both January (+1.4) and February (+1.1), with a summer average SAM anomaly of +0.8. This overall weak positive state of SAM can also be seen in Figure 10, with lower than normal pressure closer to Antarctica, and higher than normal pressure in the mid-latitudes.

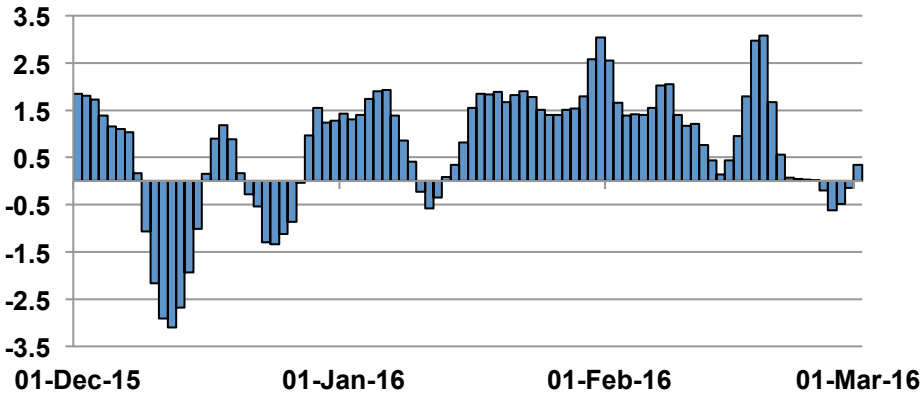

Figure 13 Summer 2015-16 daily SAM index from the Climate Prediction Center (NOAA), available from http://www.cpc.ncep.noaa.gov/products/precip/CWlink/daily_ao_index/aao/aao.shtml.

4.4 Winds

During summer 2015-16, low-level (850 hPa) winds were generally within 5 m s^{-1} of the long-term average (Figure 14). Anomalies were westerly over the equatorial Pacific, normal for El Niño years, as well as around Antarctica and the Southern Ocean, while northwesterly wind anomalies were present over Australia and the eastern Indian Ocean.

Upper-level (200 hPa) wind anomalies show enhanced easterly windflow across the equatorial Pacific and strong westerly windflow in the southern Pacific, with southwesterly wind anomalies of up to 18.8 m s^{-1} west of Peru. Windflow was also anomalously westerly in the Southern Ocean and in the equatorial Atlantic, with a clockwise gyre causing strong northwesterly flow in western Australia.

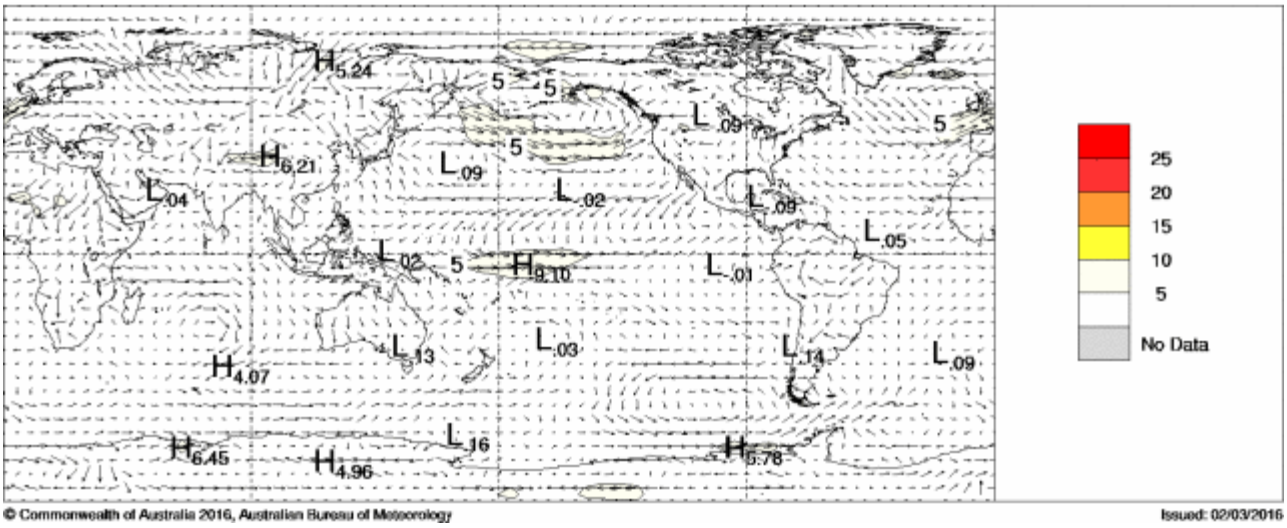

Figure 14 Summer 2015-16 850 hPa vector wind anomalies (m s^{-1}) as taken from the Bureau of Meteorology's GASP model in comparison to a 22 year NCEP2 climatology. The anomaly field is not shown over areas of elevated topography.

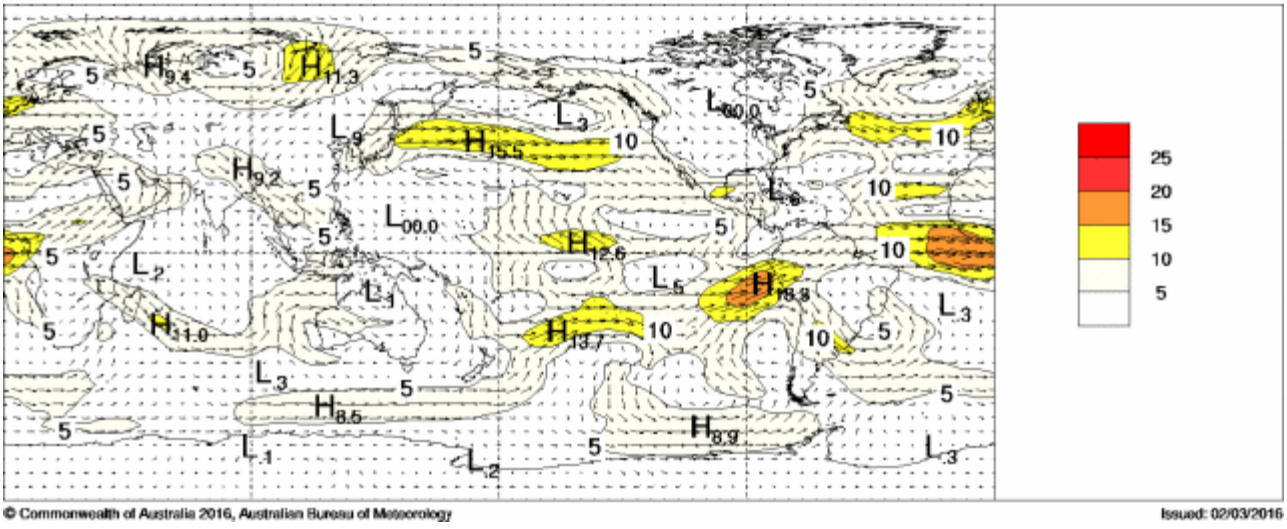

Figure 15 As in Figure 14, but for the 200 hPa winds.

5. Australian region

5.1 Rainfall

Australian summer rainfall totals for 2015-16 are shown in Figure 16, with rainfall deciles shown in Figure 17. The deciles are calculated with respect to gridded rainfall data (Jones et al. 2009) for all summers between 1900-01 and 2015-16 (i.e. 116 summers).

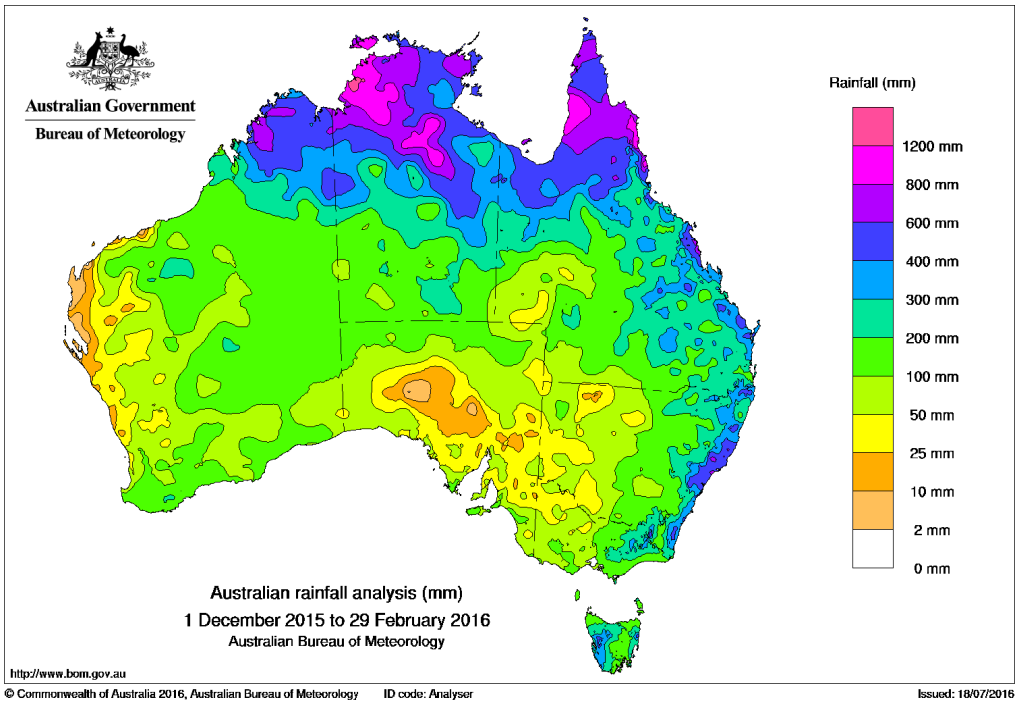

Figure 16 Summer 2015-15 rainfall totals (mm) for Australia.

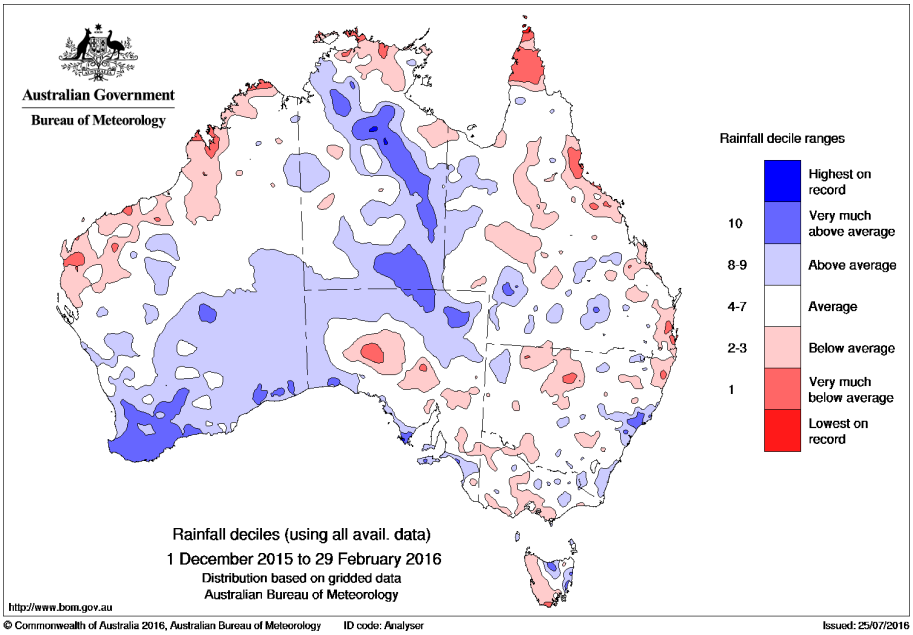

Figure 17 Summer 2015-16 rainfall deciles for Australia: decile ranges based on grid-point values over the summers 1900–2015.

Averaged across Australia, rainfall during summer 2015-16 was very close to the long-term average, with no State or Territory recording rainfall in the twenty wettest or driest summers on record (Table 1). Rainfall was well below average in parts of Far North Queensland and the Top End of the Northern Territory, consistent with the decreased convection in this region, as well as along the northwest coast of Western Australia. In comparison, rainfall was well above average in southwest Western Australia and parts of the eastern Northern Territory, with rainfall anomalies generally patchy over the remainder of the country.

The overall near-average summer rainfall hides the stark contrast between the individual months of rainfall, particularly in the north. Rainfall was well above average in northern Australia at the start of summer, with the Northern Territory recording its wettest December on record associated with a moderate MJO event and monsoon burst. In comparison, rainfall was very much below average across northern Australia during January, when rainfall was above average across much of southern and central Australia. Some parts of northeast Tasmania and southwest Western Australia experienced their wettest January on record. February featured a return to dry conditions across much of the country, with the exception of southern parts of South Australia where February rainfall was well above average.

Region	*Highest seasonal total (mm)*	*Lowest seasonal total (mm)*	*Highest daily total (mm)*	*Area-averaged rainfall (mm)*	*Rank of area-averaged rainfall*	*% difference from mean*
Australia	1630.6 at Bellenden Ker (Top)	0.0 at Urala	412.6 at Miara on 5 January	204.90	57	-1.8%
Queensland	1630.6 at Bellenden Ker (Top)	21.9 at Cameron Corner	412.6 at Miara on 5 January	281.97	37	-13.2%
New South Wales	1038.4 at Yarras	21.2 at Marra Creek	255.0 at Bungwahl on 6 January	145.31	56	-15.0%
Victoria	523.2 at Reeves Knob	14.2 at Walpa	125.0 at Carboor on 9 December	111.06	52	-7.1%
Tasmania	618.4 at Gray	81.8 at Hobart Airport	221.0 at Gray on 29 January	225.39	40	-7.3%
South Australia	195.6 at Kalamurina	2.4 at Tarcoola (Mobella)	130.8 at Kalamurina on 1 January	63.32	74	+2.1%
Western Australia	729.0 at Theda	0.0 at Urala	125.0 at Carlindie on 31 January	145.55	67	-2.5%
Northern Territory	1305.5 at Walker Creek	89.8 at Curtin Springs	291.0 at Willeroo on 26 December	375.46	84	+18.8%

Table 1 Summary of the seasonal rainfall ranks and extremes on a national and State basis for summer 2015-16. The ranking in the last column goes from 1 (lowest) to 116 (highest) and is calculated over the years 1900–2016.

5.2 Drought

By the end of summer, areas of shorter-term (ten-month and twenty-month) rainfall deficiencies in southwest Western Australia and southeast South Australia had contracted relative to deficiencies at the start of summer. However, the close to average totals resulted in little change to twenty-month and longer deficiencies in eastern parts of Victoria and Tasmania, while low rainfall resulted in the expansion of rainfall deficiencies in parts of the northern tropics. Figure 18 shows the rainfall deficiencies for the twenty months between July 2014 and February 2016, with severe rainfall deficiencies on most of central and western Victoria and western Tasmania, as well as parts of southeast South Australia, the southwest coast of Western Australia, and northern Queensland.

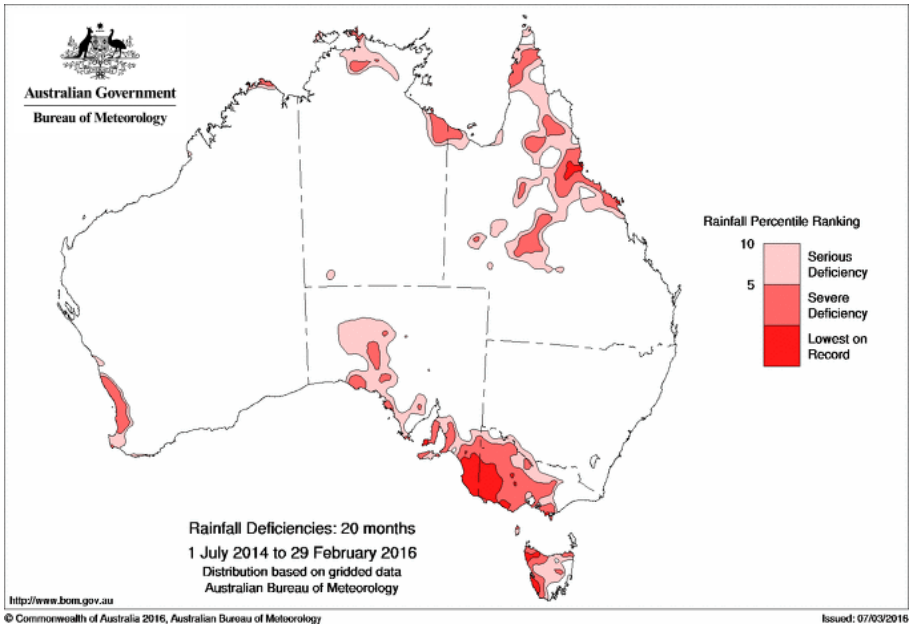

Figure 18 Rainfall deficiencies for the 20 month period 1 July 2014 to 29 February 2016

5.3 Temperature

Australian maximum and minimum temperature anomalies for summer 2015-16 are shown in Figure 19 and Figure 21. Seasonal anomalies are calculated with respect to the 1961-1990 period and use high-quality temperature reference stations from the ACORN-SAT network (Trewin 2013). Figure 20 and Figure 22 show the corresponding maximum and minimum temperature deciles, using the same gridded temperature data for all summers between 1910-11 and 2015-16.

Both maximum and minimum temperatures were warmer than average for Australia as a whole during summer 2015-16, with a mean temperature anomaly of +0.82 °C. This was the sixth-warmest summer on record for Australia, with the recent summers of 2014-15 and 2012-13 slightly warmer. Mean temperature anomalies were highest in eastern Australia, where it was the fourth-warmest summer on record.

Maximum temperatures were average to above average across most of the country, with temperatures more than 1 °C above average in most of Tasmania, Victoria, New South Wales, southern and eastern South Australia, southern Queensland, the Pilbara region of Western Australia, and the northernmost parts of Cape York, the Top End of the Northern Territory, and the Kimberley (Figure 19). Temperatures were in the warmest ten per cent of years across 18.1 per cent of the country, including all of Tasmania, most of Victoria and eastern South Australia, and parts of southern New South Wales, eastern Queensland, and the northern tropics (Figure 20. Parts of northern Tasmania recorded their warmest summer on record for maximum temperatures, with the State as a whole recording its second-warmest summer on record and the warmest since summer 1960-61 (Table 2). For Australia as a whole, summer mean maximum temperatures were the ninth-warmest on record.

The spatial pattern of minimum temperature anomalies (Figure 21) was very similar to maximum temperatures, with most of eastern Australia recording minimum temperatures more than 1 °C above average. It was the fourth-warmest summer on record for Australian minimum temperatures, with almost half the country (46.6 per cent) recording minimum temperatures in the warmest ten per cent of years. This included all of Tasmania, the Top End of the Northern Territory and the Kimberley in Western Australia, as well as most of Victoria, eastern South Australia, western New South Wales, and most of Queensland except the southeast corner (Figure 21). In parts of the country, it was the warmest summer on record, including the northern half of Tasmania. This was the warmest summer on record for Tasmania with an anomaly of +1.67 °C, 0.24 °C above the previous record (set in 1970-71). It was also the third-warmest summer on record for both Queensland and Victoria (Table 3).

Temperatures were warmest at the start of summer, with December the second-warmest on record for Australian minimum temperatures and the sixth-warmest for mean temperatures. Large areas of southeastern Australia recorded their warmest December mean temperatures on record, including the states of Tasmania, Victoria and South Australia. This was in part due to a very severe heatwave that broke records between 13 and 20 December[11]. However, parts of northern Australia experienced well below average temperatures during December associated with heavy rain. Temperatures remained broadly warmer than average in both January and February, with the exception of cooler temperatures in parts of northwest Western Australia and central Australia during January and southeast Western Australia and southern South Australia during February.

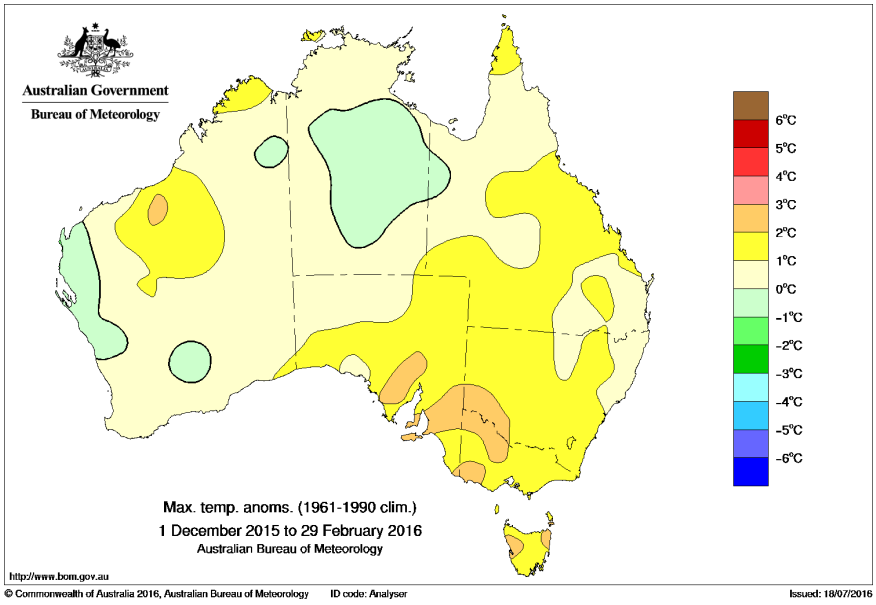

Figure 19 Summer 2015-16 maximum temperature anomalies (°C) from analysis of ACORN-SAT data.

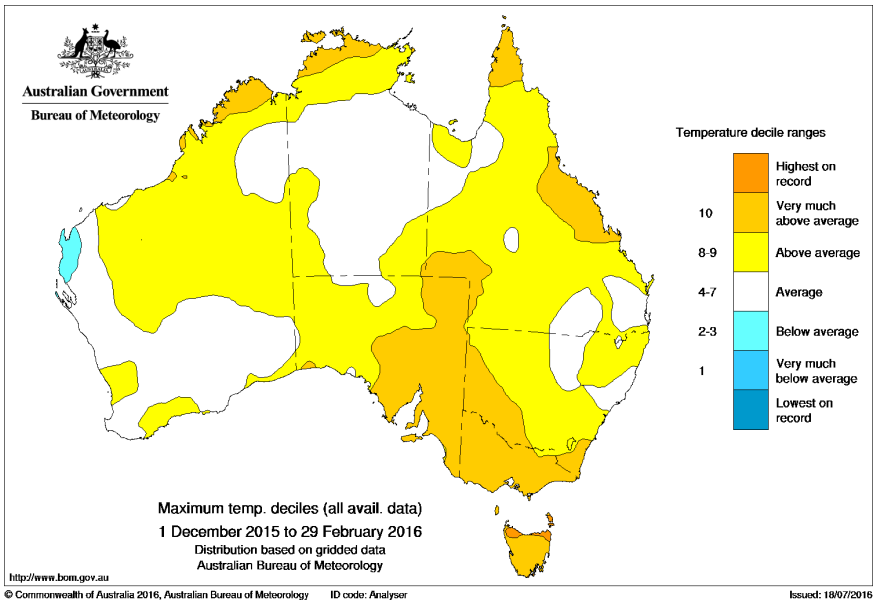

Figure 20 Summer 2015-16 maximum temperature deciles from analysis of ACORN-SAT data: decile ranges based on grid-point values over the summers 1910-2015.

[11] Information about this heatwave is given in Special Climate Statement 53: Widespread record December temperatures in southeast Australia. Available from http://www.bom.gov.au/climate/current/statements/scs53.pdf

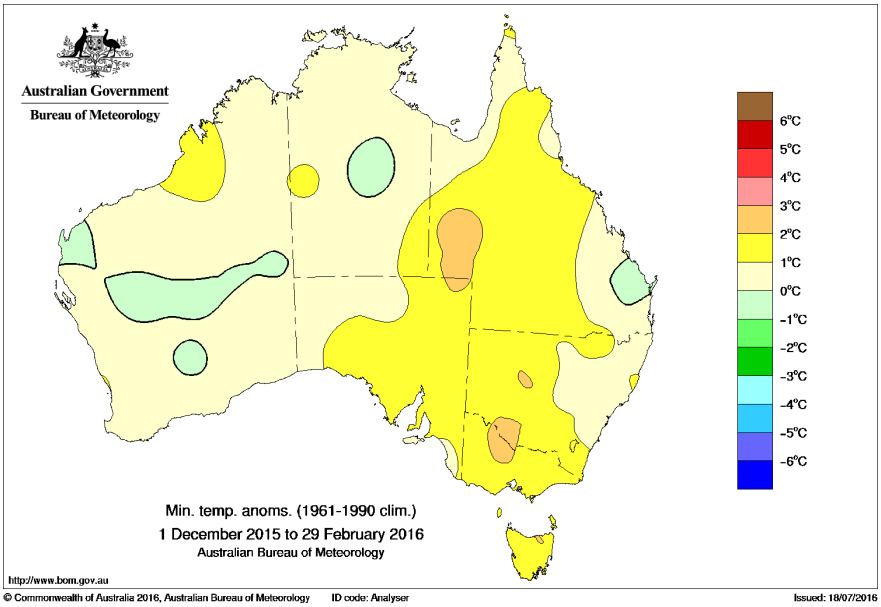

Figure 21 Summer 2015-16 minimum temperature anomalies (°C) from analysis of ACORN-SAT data.

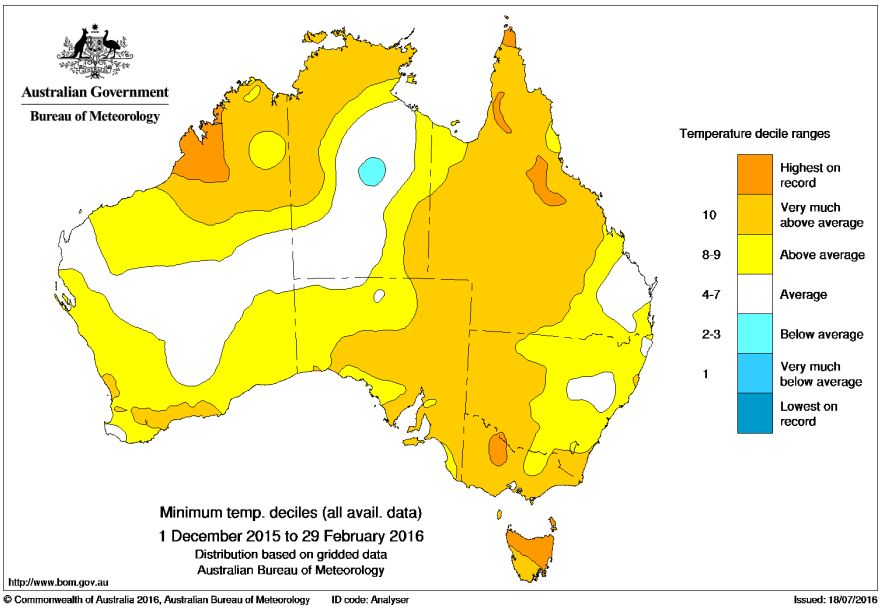

Figure 22 Summer 2015-16 minimum temperature deciles from analysis of ACORN-SAT data: decile ranges based on grid-point values over the summers 1910–2015.

Region	*Highest seasonal mean maximum (°C)*	*Lowest seasonal mean maximum (°C)*	*Highest daily temperature (°C)*	*Lowest daily maximum temperature (°C)*	*Area-averaged temperature anomaly (°C)*	*Rank of area-averaged temperature anomaly*
Australia	42.3 at Marble Bar	13.8 at kunanyi	47.8 at Mardie, 12 February, and Emu Creek, 13 February	2.6 at kunanyi on 16 February	+0.82	98
Queensland	40.0 at Birdsville	26.2 at Applethorpe	46.7 at Birdsville on 6 December	17.3 at Stanthorpe on 3 January	+0.94	90
New South Wales	37.2 at Wanaaring	15.9 at Thredbo	46.0 at Hay on 13 January	6.7 at Thredbo on 31 January	+1.43	89
Victoria	33.9 at Mildura	16.3 at Mount Hotham	45.6 at Echuca on 13 January	5.2 at Mount Baw Baw on 16 February	+1.85	103
Tasmania	25.6 at Launceston and Ouse	13.8 at kunanyi	39.8 at Friendly Beaches on 20 December	2.6 at kunanyi on 16 February	+1.89	105
South Australia	38.1 at Moomba	22.3 at Cape Willoughby	47.2 at Port Augusta on 19 December	11.7 at Mount Lofty on 1 December	+1.35	97
Western Australia	42.3 at Marble Bar	22.6 at Albany	47.8 at Mardie, 12 February, and Emu Creek, 13 February	15.6 at Shannon and Narrogin on 5 February	+0.56	90
Northern Territory	38.9 at Rabbit Flat	32.1 at McCluer Island	44.8 at Rabbit Flat on 4 January	20.9 at Arltunga on 31 December	+0.12	74

Table 2 Summary of the seasonal maximum temperature ranks and extremes on a national and State basis for summer 2015-16. The ranking in the last column goes from 1 (lowest) to 106 (highest) and is calculated over the years 1910–2016[12].

[12] A high-quality subset of the temperature network is used to calculate the spatial averages and rankings shown in Table 4 (maximum temperature) and Table 5 (minimum temperature). This dataset is known as ACORN-SAT (see http://www.bom.gov.au/climate/change/acorn-sat/ for details) These averages are available from 1910 to the present. As the anomaly averages in the tables are only retained to two decimal places, tied rankings are possible, indicated by =.

Region	*Highest seasonal mean minimum (°C)*	*Lowest seasonal mean minimum (°C)*	*Highest daily minimum temperature (°C)*	*Lowest daily temperature (°C)*	*Area-averaged temperature anomaly (°C)*	*Rank of area-averaged temperature anomaly*
Australia	27.8 at Broome	5.3 at Kunanyi	34.1 at Moomba on 7 December	-4.6 at Dinner Plain on 12 December	+0.83	103
Queensland	27.2 at Sweers Island	14.4 at Applethorpe	33.7 at Birdsville on 7 December	9.8 at Applethorpe on 19 December	+1.21	104
New South Wales	23.0 at Tibooburra	6.3 at Perisher Valley	32.2 at White Cliffs on 20 December	-3.8 at Perisher Valley on 28 December	+1.22	94
Victoria	17.6 at Mildura	7.7 at Mount Hotham	31.9 at Mildura on 20 December	-4.6 at Dinner Plain on 12 December	+1.61	104
Tasmania	15.9 at Swan Island	5.3 at Kunanyi	21.9 at Flinders Island on 20 December	-3.2 at Kunanyi on 12 December	+1.67	106
South Australia	24.4 at Moomba	11.6 at Naracoorte	34.1 at Moomba on 7 December	0.2 at Coonawarra on 2 December	+1.21	96
Western Australia	27.8 at Broome	12.9 at Rocky Gully	33.4 at Telfer on 4 January	3.2 at Jarrahwood on 25 February	+0.40	=91
Northern Territory	27.4 at McCluer Island	20.8 at Alice Springs	30.4 at Jervois on 24 December	12.0 at Kulgera on 5 and 18 February	+0.41	86

Table 3 Summary of the seasonal minimum temperature ranks and extremes on a national and State basis for summer 2015-16. The ranking in the last column goes from 1 (lowest) to 106 (highest) and is calculated over the years 1910–2016.

Acknowledgements

The author thanks Catherine Ganter and David Martin for their helpful comments on an earlier version of the manuscript.

References

Donald, A., Meinke, H., Power, B., Maia, A., de H. N., Wheeler, M.C., White, N., Stone, R.C. and Ribbe, J. (2006), Near-global impact of the Madden-Julian Oscillation on rainfall, *Geophys. Res. Lett.*, 33, L09704, doi:10.1029/2005GL025155.

Drosdowsky, W. (2005), The latitude of the subtropical ridge over Eastern Australia: The L index revisited. *Int. J. Climatol.*, 25: 1291–1299. doi:10.1002/joc.1196

Ganter, C. (2010). Seasonal climate summary southern hemisphere (winter 2010): A fast developing La Niña. *Aust. Met. Oceanogr. J.*, 61, 125–35.

Hendon, H.H., Thompson, D.W.J. and Wheeler, M.C. (2007). Australian rainfall and surface temperature variations associated with the Southern Annular Mode. *J. Clim.*, 20, 2452–2467.

Jones, D.A., Wang, W. and Fawcett, R.J. (2009). High-quality spatial climate data-sets for Australia. *Aust. Met. Oceanogr. J.*, 58, 233–248.

Kanamitsu, M., Ebisuzaki, W., Woollen, J., Yang, S.-K, Hnilo, J.J., Fiorino, M. and Potter, G.L. (2002). NCEP-DOE AMIP-II Reanalysis (R-2). *Bull. Amer. Meteor. Soc*., 83, 1631-43.

Kuleshov, Y., Qi, L., Fawcett, R. and Jones, D. (2009). "Improving preparedness to natural hazards: Tropical cyclone prediction for the Southern Hemisphere," in: Gan, J. (Ed.), *Advances in Geosciences*, Vol. 12 Ocean Science, World Scientific Publishing, Singapore, 127–43.

Lee, S.-K., Park, W., Baringer, M.O., Gordon, A.L., Huber, B. and Liu, Y. (2015). Pacific origin of the abrupt increase in Indian Ocean heat content during the warming hiatus. *Nature Geosci*., 8, 445-449, doi:10.1038/ngeo2438.

Madden, R.A. and Julian, P.R. (1971). Detection of a 40-50 day oscillation in the zonal wind in the tropical Pacific. *J. Atmos. Sci*., 28, 702–708.

Madden, R.A. and Julian, P.R. (1972). Description of global-scale circulation cells in the tropics with a 40-50 day period. *J. Atmos. Sci*., 29, 1109–1123.

Madden, R.A. and Julian, P.R. (1994). Observations of the 40-50 day tropical oscillation: a review. *Mon. Wea. Rev*., 122, 814–837.

Martin, D.J. (2016). Seasonal climate summary southern hemisphere (spring 2015): El Niño nears its peak. *J. Southern Hemisphere Earth System Science* (accepted)

Rakich, C.S., Holbrook, N.J. and Timbal, B. (2008). A pressure gradient metric capturing planetary-scale influences on eastern Australian rainfall. *Geophysical Research Letters* 35: L08713. DOI:10.1029/2007GL032970

Reynolds, R.W., Rayner, N.A., Smith, T.M., Stokes, D.C. and Wang, W. (2002). An improved in situ and satellite SST analysis for climate. *Jnl Clima*te, 15, 1609-25.

Trewin, B.C. (2013). A daily homogenised temperature dataset for Australia. *Int. J. Climatol*., 33, 1510–1529.

Troup, A.J. (1965). The Southern Oscillation. Quart. *J. Roy. Meteor. Soc*., 91, 490-506.

Wheeler, M.C. and Hendon, H. (2004). An All-Season Real-Time Multivariate MJO Index: Development of an Index for Monitoring and Prediction. *Mon. Wea. Rev*. 132, 1917–1932, doi: 10.1175/1520-0493(2004)132<1917:AARMMI>2.0.CO;2.

Wolter, K. and Timlin, M.S. (1993). Monitoring ENSO in COADS with a seasonally adjusted principal component index. Proc. Of the 17th Climate Diagnostics Workshop, Norman, OK, NOAA/NMC/CAC, NSSL, Oklahoma Clim. Survey, CIMMS and the School of Meteorology, Univ. of Oklahoma, 52-7.

Wolter, K. and Timlin, M.S. (1998). Measuring the strength of ENSO – how does 1997/98 rank? *Weather*, 53, 315-24.